NANO LETTERS

2005
Vol. 5, No. 7
1231−1236

General Route to Vertical ZnO Nanowire Arrays Using Textured ZnO Seeds

Lori E. Greene,[†] Matt Law,[†,‡] Dawud H. Tan,[†] Max Montano,[†,‡] Josh Goldberger,[†] Gabor Somorjai,[†,‡] and Peidong Yang*[,†,‡]

Department of Chemistry, University of California, Berkeley, California 94720, and Materials Sciences Division, Lawrence Berkeley National Laboratory, Berkeley, California 94720

Received April 27, 2005; Revised Manuscript Received June 2, 2005

ABSTRACT

A method for growing vertical ZnO nanowire arrays on arbitrary substrates using either gas-phase or solution-phase approaches is presented. A ~10 nm-thick layer of textured ZnO nanocrystals with their *c* axes normal to the substrate is formed by the decomposition of zinc acetate at 200–350 °C to provide nucleation sites for vertical nanowire growth. The nanorod arrays made in solution have a rod diameter, length, density, and orientation desirable for use in ordered nanorod–polymer solar cells.

Solar cells made from blends of a light-absorbing, hole-conducting polymer and an electron-accepting inorganic material are promising devices for inexpensive solar energy conversion. Typically, blended polymer−inorganic films are produced by spin coating a solution containing a mixture of a conjugated polymer and either a fullerene derivative,[1] chalcogenide nanorod,[2,3] or oxide nanocrystal[4,5] onto a transparent conducting substrate. Films made in this way can be sufficiently thick and intimately mixed to efficiently absorb light and separate charges, but they are poorly structured for efficient charge transport to the electrodes because the donor−acceptor interface is convoluted and discontinuous. In principle, a film designed to optimize charge collection would consist of a perfectly ordered array of continuous and crystalline inorganic nanorods oriented normal to the electrode surface and encased in a layer of the polymer.[6−8] To maintain efficient charge separation in a nanorod-based architecture, the rods must be thin (<40 nm) and closely spaced, with a rod-to-rod distance equal to approximately twice the diffusion length of excitons in the polymer, which is usually 5−20 nm. Zinc oxide is a nontoxic *n*-type semiconductor that has favorable band energies for forming heterojunctions with hole-conducting polymers and can be grown as nanorod arrays with the appropriate dimensions for efficient nanorod−polymer solar cells. The nanorod architecture we present here is also sufficiently open to avoid the poor polymer filling that has plagued the fabrication of cells based on nanoparticulate[9] and mesoporous titania films.[10]

High-quality vertical ZnO nanowire arrays are grown using epitaxy, either (1) heteroepitaxy with an appropriate single-crystalline substrate (usually Al_2O_3 or GaN) or (2) homoepitaxy with a textured ZnO thin film that is deposited on top of a nonepitaxial substrate (such as silicon or glass) to act as a nanowire nucleation layer. Of these two methods, heteroepitaxy is currently limited to insulating or expensive substrates,[11−13] whereas thin-film-based homoepitaxy requires gas-phase preparation of the ZnO layer[14−18] and results in a nanowire array that sits atop a disordered polycrystalline film. Neither approach is particularly low-cost, versatile, or promising for the fabrication of high-performance ZnO nanowire optoelectronic devices, including solar cells. Recently, several groups have grown vertical ZnO nanowire arrays on silicon or glass substrates without the use of a preexisting textured thin film. These arrays were synthesized at temperatures ranging from 400−600 °C using either metal−organic chemical vapor deposition (MOCVD),[19−21] pulsed laser deposition,[22] or chemical vapor transport (CVT).[23] To explain their nanorod alignment, one of the authors[23] hypothesized that a textured ZnO wetting layer formed prior to nanorod growth. If this notion is correct, it should be possible to better control the properties of this ultrathin film of textured ZnO nuclei by preparing it in a separate synthetic step. One could then create seeded surfaces for the growth of vertical ZnO nanowires on an assortment of substrates using any nanowire growth technique, gas-phase or solution-phase.

The decomposition or hydrolysis of zinc salts is an established route to the formation of ZnO colloids and nanocrystals in aqueous solution.[24−26] We adapted this approach to form layers of ZnO nanocrystals directly on a

* Corresponding author e-mail: p_yang@berkeley.edu.
[†] University of California, Berkeley.
[‡] Lawrence Berkeley National Laboratory.

10.1021/nl050788p CCC: $30.25 © 2005 American Chemical Society
Published on Web 06/18/2005

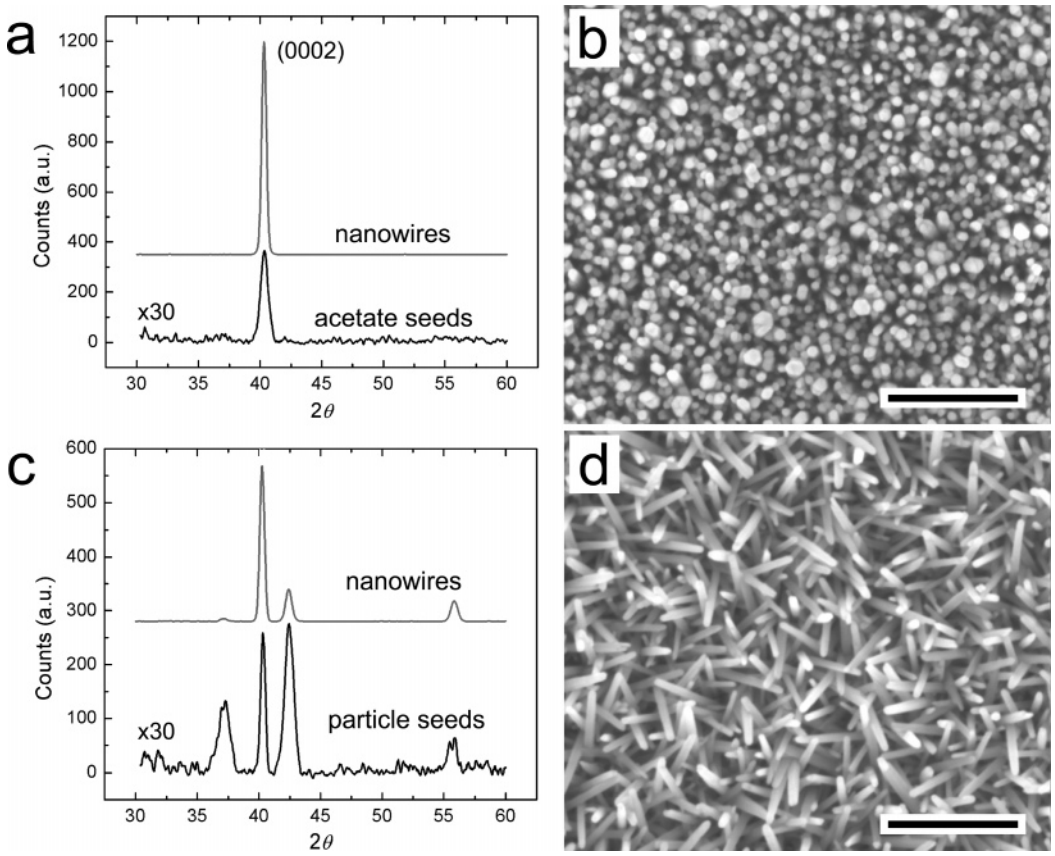

Figure 1. (a−d) Control of ZnO nanowire orientation by choice of nanoparticle seed. (a) XRD and (b) plan-view SEM data for an array grown from ZnO nanocrystal seeds that were formed in situ on a silicon surface from the decomposition of a zinc acetate precursor at 350 °C. (c) XRD and (d) SEM data for an array grown from preformed ZnO quantum dots (3−4 nm) that were dispersed onto silicon by dip-coating. Both arrays were grown for 30 min. Scale bars, 500 nm.

substrate by thermally decomposing zinc acetate at 200−350 °C. In our optimized procedure, a substrate is wet with a droplet of 0.005 M zinc acetate dihydrate (98%, Aldrich) in ethanol, rinsed with clean ethanol after 10 s, and then blown dry with a stream of argon. This coating step is repeated three to five times. The substrate, now covered with a film of zinc acetate crystallites, is heated to 350 °C in air for 20 min to yield layers of ZnO islands with their (0001) planes parallel to the substrate surface. Alignment of the ZnO nanocrystals is substrate-independent and occurs on flat surfaces regardless of their crystallinity or surface chemistry, including ZnO and Al_2O_3 single crystals, transparent conducting oxides such as indium tin oxide (ITO) and fluorine-doped tin oxide (FTO), amorphous oxides including glass and silicon with its native oxide, and the oxide-free metals gold and titanium. The zinc acetate deposition and decomposition procedure is carried out twice to ensure a complete and uniform coverage of ZnO seeds.

We grew vertical ZnO nanorod arrays from the aligned nanocrystal seeds in aqueous solution at 90 °C.[27,28] Figure 1 compares a nanorod array grown from the aligned acetate-derived seeds with another array seeded with preformed ZnO nanocrystals[29] that were dip-coated onto the substrate surface. X-ray diffraction (XRD) was performed on both seeded substrates before and after wire growth. Prior to growth, the aligned seeds show only a (0002) reflection, indicating their complete *c*-axis texturing, whereas the dip-coated seeds give a powder pattern because they rest at all angles on the substrate. XRD patterns of the resulting nanorod arrays demonstrate that the orientation of the ZnO seeds directly determines the orientation of the nanorods. Although silicon substrates are used here for ease of imaging, we routinely obtain completely vertical rod arrays over the entire surface of any of the substrates mentioned above. See Figure S1 of the Supporting Information for a plan-view image of vertical array on ITO grown by the same aqueous method.

These vertical nanorod arrays are highly suitable for use in ordered nanorod−polymer solar cells. First, the rod diameter, length, spacing, and orientation are appropriate for forming a high-performance bulk heterojunction by filling the vertical array with a semiconducting polymer. Figure 2a is a tilted SEM image of an array grown on silicon in aqueous solution, whereas Figure 2b shows a similar array in cross-section. Both arrays consist of nanorods with diameters of 15−65 nm and lengths of 250−400 nm, separated by gaps of 5−45 nm (see also Figure S1). The nanorod number density can be as high as 70 billion rods per square centimeter. These geometric parameters are tunable to varying degrees by changing the growth time, solution composition, or seed density. For example, the nanorod length increases linearly with growth time and can be tuned from 100 to 1200 nm before the rods begin to coalesce. Second, the rods grow directly from the substrate without an intermediate thin film of ZnO that might complicate

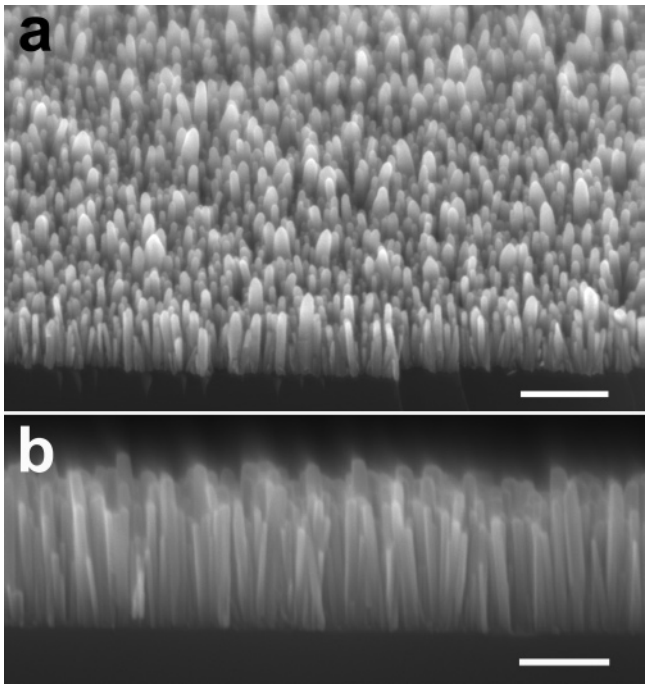

Figure 2. SEM characterization of vertical nanowire arrays on silicon. (a) Image taken at a 45° tilt. Wire lengths and diameters are 250−400 nm and 15−65 nm, respectively. Scale bar, 500 nm. (b) Cross-sectional image of a different array showing the absence of an intermediate nanoparticle layer. Scale bar, 200 nm.

electron transport. Our ZnO rod arrays form ohmic junctions with ITO; two-point electrical measurements give linear current−voltage ($I-V$) traces similar to recent measurements on nanowire arrays produced from preformed seeds.[28] The ZnO rod arrays are filled easily with hole-conducting polymers such as poly(3-hexylthiophene) to yield functioning solar cells.[30]

The aligned ZnO seeds were characterized with transmission electron microscopy (TEM) and scanning tunneling microscopy (STM) to better understand their microstructure and mechanism of formation. For TEM studies, acetate-derived seeds were grown directly on a TEM membrane window grid (50-nm-thick Si_3N_4 window, ∼2 nm RMS roughness, SPI Supplies) using only one deposition−decomposition cycle to ensure a relatively low seed density. Figure 3a is a lattice-resolved image of a single ZnO seed on the TEM window. The labeled lattice directions correspond to the perpendicular $\{10\bar{1}0\}$ and $\{11\bar{2}0\}$ planes of ZnO, confirming that the *c* axis is normal to the membrane surface. Weak hexagonal faceting of the seed is also evident. Low-magnification TEM images (not shown) indicate that the seeds are fairly uniform in size with diameters of 5−15 nm. Selected area electron diffraction (SAED) was utilized at low magnification to investigate the alignment of the seed ensemble. The polycrystalline diffraction pattern in Figure 3b lacks the (0002) ring, as expected for seeds with strong *c*-axis texturing normal to the membrane and no in-plane rotational alignment.

For STM studies, acetate-derived seeds were formed in situ on flat ITO substrates (<1 nm RMS roughness, Thin Film Devices, Inc.) using two deposition−decomposition

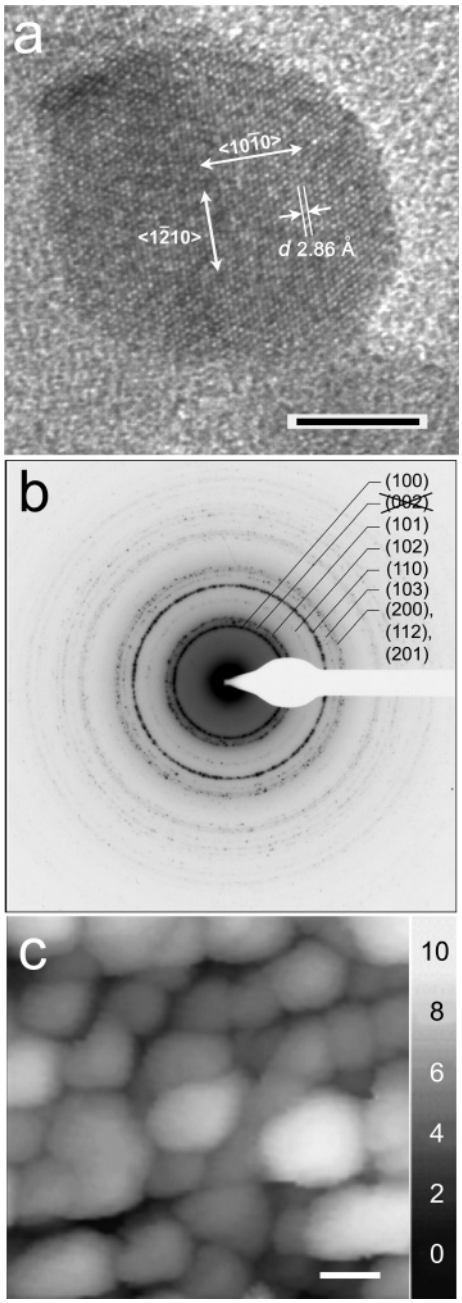

Figure 3. Characterization of the acetate-derived ZnO seeds made at 350 °C. (a) TEM image of a single seed grown on the surface of a flat, electron-transparent Si_3N_4 membrane. The labeled distance of 2.86 Å corresponds to the $\{10\bar{1}0\}$ lattice spacing. Scale bar, 6 nm. (b) Electron diffraction of an ensemble of seeds on the same nitride window. The (0002) ring is missing from the pattern, consistent with strong *c*-axis texturing of the seeds. (c) STM topographic image of a seed layer on ITO. The points of minimal height correspond to the ITO surface, which was confirmed by imaging samples with a lower seed density to allow a clear view of the underlying substrate. Height bar is in units of nanometers. Scan parameters: 100 mV and 200 pA. Scale bar, 10 nm.

cycles. STM topography images (Figure 3c) show that the seeds are relatively flat platelets with diameters of 5−20 nm and thicknesses of 3−5 nm. The average diameter of the seeds is somewhat larger than was found in TEM, probably as a result of STM tip convolution. Structurally, a film with a maximum thickness of about 10 nm is formed from two

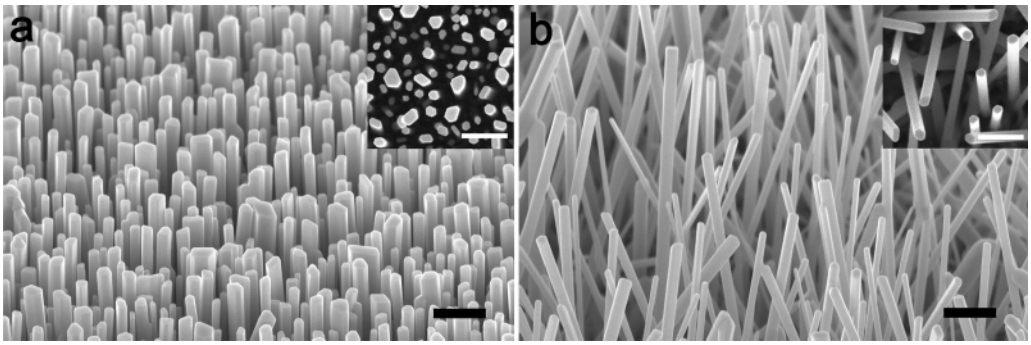

Figure 4. Gas-phase growth of oriented ZnO nanowires on nonepitaxial substrates. (a) ZnO nanowires grown on a silicon (100) surface from acetate-derived seeds; image taken at a 45° tilt. Inset is a plan-view image. (b) ZnO nanowires grown on the same surface without seeds (but with gold catalyst), imaged at a 45° tilt. Inset is a plan-view image. All scale bars are one micron.

to three seed layers, which is consistent with SEM measurements that fail to resolve a particle layer at the base of the nanorods. The combined XRD, TEM, and STM data strongly suggest that *c*-axis texturing occurs across the ZnO seed multilayer.

This aligned seeding strategy is compatible with any ZnO nanowire growth method, including gas-phase techniques. As an illustration, we used a gold-catalyzed carbothermal reduction method[31] to grow ZnO wires on silicon (100) substrates at 900 °C. Figure 4 compares arrays made from substrates with and without acetate-derived seeds. Both substrates were coated with 20 Å of gold immediately before nanowire growth. While the unseeded substrate yielded a disordered wire array, as one would expect for nonepitaxial ZnO growth on silicon, the seeded substrate produced vertical wires (see also Figure S2). Vertical wire arrays were also grown from seeded substrates without the gold film. These gas-phase wires grow to significantly larger diameters at a lower density than the solution-phase wires, perhaps because of different growth mechanisms or seed aggregation at high temperature. We note that control experiments using substrates with neither seeds nor gold showed no nanowire growth.

We now examine the reason for the *c*-axis alignment of the acetate-derived ZnO seeds. As a reminder, the polar {0001} faces of wurtzite ZnO are electrostatically unstable Tasker type III surfaces[32] that cannot exist without a mechanism to redistribute their surface charge and lower their free energy. Polar surfaces are generally stabilized in one of three ways:[33] (1) surface reconstruction or faceting; (2) the transfer of charge between surfaces (i.e., electronic relaxation); or (3) surface nonstoichiometry, including the neutralization of surface charge by adsorbed molecules. The {0001} facets of ZnO have been studied heavily both experimentally and theoretically to clarify the operative stabilization mechanisms, especially after it was pointed out[34] that neither surface reconstructs (which rules out the most common stabilization pathway, mechanism 1).

We summarize the results of these studies here as a point of reference. Ab initio calculations performed for perfect ZnO{0001} facets consistently find that stability is achieved by an exchange of charge mediated by surface states (mechanism 2).[35−38] According to these models, optimized {0001} surfaces have roughly a 60% higher cleavage energy[39] than the nonpolar $\{10\bar{1}0\}$ and $\{11\bar{2}0\}$ faces, independent of the specific functional used in the calculations. However, surface-sensitive spectroscopic studies[40,41] show no evidence for substantial charge transfer on real ZnO-{0001} faces, calling the relevance of the theoretical findings into question. Scanning tunneling microscopy has shown that clean (0001)-Zn faces roughen across two atomic layers in order to stabilize themselves by nonstoichiometry (mechanism 3);[41,42] adsorbates may also be involved. Stabilization of the $(000\bar{1})$-O facet is more controversial. When clean, this surface is unambiguously atomically flat and stoichiometric. Recent ion-scattering evidence suggests that adsorbed hydrogen is important for charge neutralization on the $(000\bar{1})$-O face,[43,44] but other studies dispute this possibility,[41] and the problem is unresolved. Experiments have thus far yielded no reliable quantitative information on the energies of the various ZnO surfaces, perfect or otherwise.

If the ZnO{0001} faces are the highest-energy low-index planes, as theory claims, we face an immediate problem in explaining the dominance of *c*-axis texturing in ZnO islands, thin films, and nanowires. ZnO films deposited at elevated temperatures are usually oriented with the *c* axis perpendicular to the substrate surface, even on amorphous substrates such as glass. Moreover, single-crystalline ZnO nanowires synthesized without the use of epitaxy almost always grow along the *c* direction, regardless of growth method (gas- or solution-phase). These growth habits suggest that the *c* axis is the fastest growth direction and therefore that ZnO{0001} is the highest-energy of the low-index surfaces, in agreement with theory. It is reasonable to expect that ZnO film/wire orientation is determined by the nucleation and growth of the first few layers of zinc and oxygen atoms. How does *c*-axis texture develop in these initial nuclei when the {0001} planes are higher in energy than other ZnO surfaces?

Our acetate-derived ZnO seeds provide an important new example of *c*-axis alignment. Each seed is a relatively flat platelet that is 25−40 atomic layers thick. Because seed alignment occurs on disparate, nonepitaxial surfaces, ZnO-substrate interactions are probably not an important driving force for texturing. Instead, texturing seems to be an intrinsic thermodynamic feature of the growth of these nuclei. We propose three mechanisms that could enable the *c*-axis

texturing of nucleating ZnO seeds despite the high energy of the {0001} surfaces: (1) molecules present under the experimental conditions adsorb onto nascent {0001} surfaces and stabilize them relative to competing facets. In the decomposition of zinc acetate to ZnO, these adsorbates would be primarily acetate and hydroxyl groups. (2) The {0001} surface energy depends on the crystal thickness so that very thin ZnO crystals prefer a {0001} orientation, which is then kinetically locked-in as growth proceeds. Calculations on isolated ZnO slabs show that the {0001} cleavage energy does decrease as a slab is made thinner, but probably not enough to drop below the energies of the nonpolar faces. (3) The first few atomic layers of ZnO adopt a low-energy configuration different from the bulk lattice and later convert to the (0001) orientation by a minor structural transformation. Claeyssens et al. found recently that extremely thin ZnO films may exist in a graphitic arrangement that undergoes a barrierless transition to the (0001) morphology above a threshold thickness of 10−20 Å.[38] If this type of mechanism is confirmed by future investigations, it may have implications for the *c*-axis orientation of wurtzite thin films and nanowires in general.

The microscopic details of seed formation are not sufficiently understood to pinpoint which, if any, of the above mechanisms is responsible for seed alignment. Thermogravimetry and differential thermal analysis of zinc acetate dihydrate show that this solid begins to sublime at ∼175 °C, melts at ∼250 °C and converts completely to ZnO by 350 °C (Figure S3). To ascertain the minimum temperature required to form textured seeds from zinc acetate, we grew nanorod arrays from seeds prepared at 300, 250, 200, and 150 °C. Lowering the preparation temperature from 350 to 200 °C results in vertical arrays of progressively thinner nanorods (Figure S4). Our alignment strategy begins to fail for preparation temperatures lower than 200 °C. Nanorods grown from acetate-derived seeds made at 150 °C are poorly aligned compared to those produced above 200 °C (Figure S5). Preparation temperatures lower than 100 °C cause seeding itself to fail because the zinc acetate crystallites simply dissolve into the nanorod growth bath. These experiments suggest that temperatures between 150 and 200 °C are needed for seed alignment, whereas higher temperatures promote mainly seed crystallinity and growth.

We tested two additional zinc compounds to determine whether zinc acetate is unique in its tendency to form textured oxide islands. Seeds grown in situ at 350 °C from zinc acetylacetonate or zinc nitrate hexahydrate yielded unaligned nanorods (Figure S6), even though both solids decompose to ZnO below this temperature (Figure S7). The texturing of the acetate-derived seeds must therefore stem from either the particular kinetics of zinc acetate decomposition or the specific adsorbates present during its conversion to ZnO islands.

We have presented a simple seeding method for producing vertical ZnO nanowire arrays on any flat substrate that can survive heat treatments at 200 °C or greater. By forming layers of aligned ZnO nanocrystals in situ on a substrate, we create a surface that can be paired with nearly any ZnO growth technique, gas-phase or solution-phase, to fabricate high-density vertical wire arrays free of intermediate thin films or nanoparticle layers. The arrays grown from aqueous solution feature a nanorod diameter, length, density, and orientation that make them highly suitable as the inorganic scaffold in efficient nanorod−polymer solar cells.

Acknowledgment. This work was supported by the Department of Energy, Office of Basic Sciences. M.L. is a Berkeley-ITRI Fellow. We thank R. Brutchey for help with TG/DTA.

Supporting Information Available: Supporting figures S1−S7, including SEM and thermal analysis data. This material is available free of charge via the Internet at http://pubs.acs.org.

References

(1) Padinger, F.; Rittberger, R. S.; Sariciftci, N. S. *Adv. Funct. Mater.* **2003**, *13*, 85−88.
(2) Huynh, W. U.; Dittmer, J. J.; Alivisatos, A. P. *Science* **2002**, *295*, 2425−2427.
(3) Sun, B.; Marx, E.; Greenham, N. C. *Nano Lett.* **2003**, *3*, 961−963.
(4) Kwong, C. Y.; Choy, W. C. H.; Djurišić, A. B.; Chui, P. C.; Cheng, K. W.; Chan, W. K. *Nanotechnology* **2004**, *15*, 1156−1161.
(5) Beek, W. J. E.; Wienk, M. M.; Janssen, R. A. J. *Adv. Mater.* **2004**, *16*, 1009−1013.
(6) Kannan, B.; Castelino, K.; Majumdar, A. *Nano Lett.* **2003**, *3*, 1729−1733.
(7) Coakley, K. M.; McGehee, M. D. *Chem. Mater.* **2004**, *16*, 4533−4542.
(8) Mehta, B. R.; Kruis, F. E. *Sol. Energy Mater. Sol. Cells* **2005**, *85*, 107−113.
(9) Ravirajan, P.; Haque, S. A.; Durrant, J. R.; Poplavskyy, D.; Bradley, D. D. C.; Nelson, J. *J. Appl. Phys.* **2004**, *95*, 1473−1480.
(10) Coakley, K. M.; McGehee, M. D. *Appl. Phys. Lett.* **2003**, *83*, 3380−3382.
(11) Huang, M. H.; Mao, S.; Feick, H.; Yan, H.; Wu, Y. Y.; Kind, H.; Weber, E.; Russo, R.; Yang, P. *Science* **2001**, *292*, 1897−1899.
(12) Park, W. I.; Kim, D. H.; Jung, S.-W.; Yi, G.-C. *Appl. Phys. Lett.* **2002**, *80*, 4232−4234.
(13) Yan, M.; Zhang, H. T.; Widjaja, E. J.; Chang, R. P. H. *J. Appl. Phys.* **2003**, *94*, 5240−5246.
(14) Henley, S. J.; Ashfold, M. N. R.; Nicholls, D. P.; Wheatley, P.; Cherns, D. *Appl. Phys. A* **2004**, *79*, 1169−1173.
(15) Peterson, R. B.; Fields, C. L.; Gregg, B. A. *Langmuir* **2004**, *20*, 5114−5118.
(16) Hung, C.-H.; Whang, W.-T. *J. Cryst. Growth* **2004**, *268*, 242−248.
(17) Wang, L.; Zhang, X.; Zhao, S.; Zhou, G.; Zhou, Y.; Qi, J. *Appl. Phys. Lett.* **2005**, *86*, 024108.
(18) Li, Q.; Kumar, V.; Li, Y.; Zhang, H.; Marks, T. J.; Chang, R. P. H. *Chem. Mater.* **2005**, *17*, 1001−1006.
(19) Park, W. I.; Yi, G.-C.; Kim, M.; Pennycook, S. J. *Adv. Mater.* **2002**, *14*, 1841−1843.
(20) Wu, J.-J.; Liu, S.-C. *Adv. Mater.* **2002**, *14*, 215−218.
(21) Yuan, H.; Zhang, Y. *J. Cryst. Growth* **2004**, *263*, 119−124.
(22) Sun, Y.; Fuge, G. M.; Ashfold, M. N. R. *Chem. Phys. Lett.* **2004**, *396*, 21−26.
(23) Zhang, H. Z.; Sun, X. C.; Wang, R. M.; Yu, D. P. *J. Cryst. Growth* **2004**, *269*, 464−471.
(24) Meulenkamp, E. A. *J. Phys. Chem. B* **1998**, *102*, 5566−5572.
(25) Sakohara, S.; Ishida, M.; Anderson, M. A. *J. Phys. Chem. B* **1998**, *102*, 10169−10175.
(26) McBride, R. A.; Kelly, J. M.; McCormack, D. E. *J. Mater. Chem.* **2003**, *13*, 1196−1201.
(27) Greene, L. E.; Law, M.; Goldberger, J.; Kim, F.; Johnson, J. C.; Zhang, Y.; Saykally, R. J.; Yang, P. *Angew. Chem., Int. Ed.* **2003**, *42*, 3031−3034.
(28) Law, M.; Greene, L. E.; Goldberger, J.; Johnson, J. C.; Saykally, R. J.; Yang, P. *Nature Mater.* **2005**, *4*, 455−459.
(29) Pacholski, C.; Kornowski, A.; Weller, H. *Angew. Chem., Int. Ed.* **2002**, *41*, 1188−1191.

(30) Law, M.; Greene, L. E.; Yang, P. Unpublished results.
(31) Yang, P.; Yan, H.; Mao, S.; Russo, R.; Johnson, J.; Saykally, R.; Morris, N.; Pham, J.; He, R.; Choi, H.-J. *Adv. Funct. Mater.* **2002**, *12*, 323−331.
(32) Tasker, P. W. *J. Phys. C* **1979**, *12*, 4977−4984.
(33) Noguera, C. *J. Phys.: Condens. Matter* **2000**, *12*, R367 − R410.
(34) Nosker, R. W.; Mark, P.; Levine, J. D. *Surf. Sci.* **1970**, *19*, 291−317.
(35) Wander, A.; Schedin, F.; Steadman, P.; Norris, A.; McGrath, R.; Turner, T. S.; Thornton, G.; Harrison, N. M. *Phys. Rev. Lett.* **2001**, *86*, 3811−3814.
(36) Meyer, B.; Marx, D. *Phys. Rev. B* **2003**, *67*, 035403.
(37) Diebold, U.; Koplitz, L. V.; Dulub, O. *Appl. Surf. Sci.* **2004**, *237*, 336−342.
(38) Claeyssens, F.; Freeman, C. L.; Allan, N. L.; Sun, Y.; Ashford, M. N. R.; Harding, J. H. *J. Mater. Chem.* **2005**, *15*, 139−148.
(39) There is no unique surface energy for the polar (000$\bar{1}$)-O and (0001)-Zn faces because cleavage of the crystal produces both surfaces simultaneously. The surface energy of a nonpolar surface is simply half of its cleavage energy.
(40) Girard, R. T.; Tjernberg, O.; Chiaia, G.; Söderholm, S.; Karlsson, U. O.; Wigren, C.; Nylén, H.; Lindau, I. *Surf. Sci.* **1997**, *373*, 409−417.
(41) Dulub, O.; Boatner, L. A.; Diebold, U. *Surf. Sci.* **2002**, *519*, 201−217.
(42) Dulub, O.; Diebold, U.; Kresse, G. *Phys. Rev. Lett.* **2003**, *90*, 016102.
(43) Kunat, M.; Girol, S. G.; Becker, T.; Burghaus, U.; Wöll, C. *Phys. Rev. B* **2002**, *66*, 081402(R).
(44) Staemmler, V.; Fink, K.; Meyer, B.; Marx, D.; Kunat, M.; Girol, S. G.; Burghaus, U.; Wöll, C. *Phys. Rev. Lett.* **2003**, *90*, 106102.

NL050788P